A decision support system for selection and risk management of sustainability governance approaches in multi-tier supply chain

Jamalnia, Aboozar; Gong, Yu; Govindan, Kannan; Bourlakis, Michael; Mangla, Sachin Kumar

Published in:
International Journal of Production Economics

DOI:
10.1016/j.ijpe.2023.108960

Publication date:
2023

Document version:
Final published version

AGU ADVANCING EARTH AND SPACE SCIENCES

Geophysical Research Letters®

RESEARCH LETTER
10.1029/2023GL103109

Disentangling Effects of Sea Surface Temperature and Water Depth on Hydroxylated Isoprenoid GDGTs: Insights From the Hadal Zone and Global Sediments

Wenjie Xiao[1,2], Yunping Xu[3], Chuanlun Zhang[1,4,5], Jian Lin[1,4,6], Weichao Wu[3], Xiaoxia Lü[7], Jingqian Tan[1], Xi Zhang[3], Fengfeng Zheng[1], Xiuqing Song[5], Yuanqing Zhu[1,5], Yi Yang[7], Hongrui Zhang[8], Frank Wenzhöfer[2,9,10], Ashley A. Rowden[11,12], and Ronnie N. Glud[2,13]

[1]Shenzhen Key Laboratory of Marine Archaea Geo-Omics, Department of Ocean Science and Engineering, Southern University of Science and Technology, Shenzhen, China, [2]Department of Biology, HADAL, Nordcee & DIAS, University of Southern Denmark, Odense M, Denmark, [3]Shanghai Frontiers Research Center of the Hadal Biosphere & HAST, College of Marine Sciences, Shanghai Ocean University, Shanghai, China, [4]Southern Marine Science and Engineering Guangdong Laboratory (Guangzhou), Guangzhou, China, [5]Shanghai Sheshan National Geophysical Observatory, Shanghai, China, [6]Key Laboratory of Ocean and Marginal Sea Geology, Chinese Academy of Sciences, Guangzhou, China, [7]Hubei Key Laboratory of Marine Geological Resource, China University of Geosciences, Wuhan, China, [8]Department of Earth Sciences, ETH Zurich, Zurich, Switzerland, [9]HGF-MPG Group for Deep Sea Ecology & Technology, Alfred Wegener Institute Helmholtz Centre for Polar- and Marine Research, Bremerhaven, Germany, [10]Max Planck Institute for Marine Microbiology, Bremen, Germany, [11]Coast and Oceans National Centre, National Institute of Water & Atmosphere Research (NIWA) Ltd, Wellington, New Zealand, [12]School of Biological Sciences, Victoria University of Wellington, Wellington, New Zealand, [13]Department of Ocean and Environmental Sciences, Tokyo University of Marine Science and Technology, Tokyo, Japan

Abstract Hydroxylated isoprenoid glycerol dialkyl glycerol tetraethers (OH-GDGTs) preserved in marine sediments are thought to be controlled by sea surface temperature (SST). However, water depth may also exert a significant influence on OH-GDGTs. Here, we investigated sedimentary OH-GDGTs in the Kermadec and Atacama trench regions (2,560–9,560 m water depth). Sedimentary OH-GDGTs in hadal trenches were dominated by OH-GDGT-0 (72 ± 8%), potentially reflecting an adaption of source organisms to ambient cold deep water. This result, combined with global data set, revealed that the predominance of OH-GDGT-0 is a ubiquitous phenomenon in deep-sea sediments, leading to a considerable underestimation of RI-OH′-derived SSTs. By considering both SST and water depth effects, we developed more accurate OH-GDGT-based paleothermometers for both shallow regions and the global ocean, encompassing the full-ocean-depth range. Our findings highlight the importance of accounting for the effect of water depth on OH-GDGTs and provide improved tools for reconstructing paleo-SSTs.

Plain Language Summary Building quantitative proxies that can accurately estimate SSTs is one of the most common themes in paleoceanography. Archeal-derived hydroxylated isoprenoid glycerol dialkyl glycerol tetraethers (OH-GDGTs) preserved in marine sediments have a potential to reflect past sea surface temperatures (SSTs). However, the source organisms of OH-GDGTs can live throughout the water column, implying that sedimentary OH-GDGTs record an integrated water column signal rather than only SST. Currently, the effect of water depth on sedimentary OH-GDGTs remains vague. We investigated the distribution of OH-GDGTs in 13 sediment cores in the hadal zone, which represents the deepest and least explored habitats on Earth's surface. The data from this study and literature revealed that the deep-sea (including hadal trench) sediments are characterized by a predominance of OH-GDGT-0, which causes a considerable underestimation of OH-GDGT-derived SSTs. We evaluated the effects of both SST and water depth on OH-GDGTs and established new calibrations that more accurately reconstruct paleotemperatures at a global scale.

Key Points:

- Sedimentary hydroxylated isoprenoid glycerol dialkyl glycerol tetraethers (OH-GDGTs) were first investigated in the Kermadec and Atacama trenches with water depth ranging from 2,560 to 9,560 m
- Water depth has large impact on OH-GDGT distributions with higher OH-GDGT-0% and lower RI-OH′ values of deep-sea sediments
- More accurate global sea surface temperature calibrations based on OH-GDGTs were established

Supporting Information:

Supporting Information may be found in the online version of this article.

Correspondence to:

W. Xiao and C. Zhang,
wjxiaocug@126.com;
zhangcl@sustech.edu.cn

Citation:

Xiao, W., Xu, Y., Zhang, C., Lin, J., Wu, W., Lü, X., et al. (2023). Disentangling effects of sea surface temperature and water depth on hydroxylated isoprenoid GDGTs: Insights from the hadal zone and global sediments. *Geophysical Research Letters*, *50*, e2023GL103109. https://doi.org/10.1029/2023GL103109

Received 1 FEB 2023
Accepted 13 JUL 2023

1. Introduction

Accurately quantifying sea surface temperature (SST) is of great importance to understand oceanic heat transport and the Earth's climate sensitivity. Molecular biomarkers preserved in marine sedimentary archives record information on the growth environment of the source organisms, and thus serve as essential tools for paleotemperature reconstructions (Summons et al., 2022). Of these, archeal cell membrane lipids characterized by isoprenoid glycerol dialkyl glycerol tetraethers (isoGDGTs) have received considerable attention because isoGDGTs

are ubiquitously distributed in marine sediments, and are applicable over geological time spanning up to Early Jurassic (Robinson et al., 2017; Schouten et al., 2013). Based on the relative abundance of cyclopentane rings of isoGDGTs, the TetraEther indeX of 86 carbons (TEX_{86}) has been developed. TEX_{86} shows a strong relationship with SST using the global core-top data set, and has been employed in numerous paleo-studies over the past two decades (Inglis & Tierney, 2020; Rattanasriampaipong et al., 2022; Schouten et al., 2013).

Besides isoGDGTs, a new suite of GDGTs called OH-GDGTs, are also identified in marine sediments (X. Liu et al., 2012). OH-GDGTs such as OH-GDGT-0, 1, and 2 contain 0-2 cyclopentane rings with 1 hydroxyl group positioned at one of the two biphytanyl chains (Figure 1a). OH-GDGTs in marine sediments are thought to be primarily derived from planktonic Thaumarchaeota, which is supported by being only present in Thaumarchaeota Group 1.1a, and absent in strains falling into Group 1.1b in culture experiments (Elling et al., 2014, 2017). However, the occurrence of OH-GDGTs in a thermophilic euryarcheon suggests that multiple sources are possible (M. Liu et al., 2012).

Huguet et al. (2013) found that the contribution of OH-GDGTs to the total isoGDGT pool correlated with increasing latitude and decreasing SST. Fietz et al. (2013) suggested that the relative number of cyclopentane rings of OH-GDGTs, similar to that of isoGDGTs, could also reflect SSTs. Lü et al. (2015) proposed two Ring Indexes of OH-GDGTs (namely RI-OH and RI-OH′; see Equations 2 and 3 in Section 2.4) based on the weighted average number of cyclopentane rings of OH-GDGTs. RI-OH and RI-OH′ have been applied to reconstruct SSTs in diverse marine environments (Davtian & Bard, 2023; Davtian et al., 2019, 2021; Fietz et al., 2016; Kremer et al., 2018; Morcillo-Montalba et al., 2021; Sinninghe Damste et al., 2022). Besides water temperature, other factors like water salinity (Sinninghe Damste et al., 2022), dissolved oxygen and nitrate (Harning et al., 2023), sea ice (Fietz et al., 2013), seasonality (Lü et al., 2019) and terrestrial input (Kang et al., 2017; Wei et al., 2020) may also affect the distribution of OH-GDGTs in marine sediments.

However, the ecophysiology of OH-GDGT-producing organisms, mainly Thaumarchaeota, remain elusive. Thaumarchaeota can live throughout the water column, and are thought to be subdivided into "shallow" (i.e., <200 m) and "deep water" (i.e., >1,000 m) clusters (Villanueva et al., 2015). The contribution of isoGDGTs from the latter could be incorporated into the sedimentary isoGDGT pool, causing a bias in reconstructed TEX_{86} SST estimates (Kim et al., 2015; Rattanasriampaipong et al., 2022). In this perspective, OH-GDGT-based proxies may also record integrated water column temperature rather than surface temperature. Thus, the application of previously defined OH-GDGT-based proxies to estimate SSTs should consider the water depth effect. Studies for the East China Sea (Lü et al., 2019) and South China Sea (Yang et al., 2018) have shown that the composition and distribution of OH-GDGTs varied with increasing water depth. However, the effect of water depth on OH-GDGT-based proxies has sparsely been evaluated.

The hadal zone, comprising the water depth of 6,000–11,000 m, is the deepest part of the world's oceans (Glud et al., 2013). It is mainly composed of oceanic trenches formed by subduction at tectonic convergence zones (Stewart & Jamieson, 2018). The hadal zone remains one of the least understood habitats on Earth, representing the last major marine ecological frontier (Xu et al., 2018). To date, few studies have reported archeal isoGDGTs and bacterial branched GDGTs in the hadal zone (e.g., Xiao et al., 2020a; Xu et al., 2020a), and only one study reported OH-GDGTs in the Mariana and Yap trenches (Chen et al., 2020) which showed that the fractional abundance of acyclic OH-GDGTs increased with increasing water depth. The extreme water depth makes the hadal zone an ideal area to test the applicability of OH-GDGT-based proxies in deep oceans. Here, we investigated OH-GDGT distributions in 176 sediment samples in 13 sediment cores from the Atacama and Kermadec trench regions. By compiling a data set comprising globally distributed marine samples, we aim to: (a) determine the composition and distribution of OH-GDGTs in the deepest ocean sediments; (b) evaluate the relative importance of water depth on the distribution of OH-GDGTs at a full-ocean-depth range; and (c) establish more robust OH-GDGT-based proxies to estimate SSTs at a global scale.

2. Materials, Methods, and Data Compilation

2.1. Sample Collection

Sediment cores were retrieved from Kermadec and Atacama trench regions (Text S1 in Supporting Information S1) during two cruises aboard on *R/V Tangaroa* (November to December 2017) and *R/V Sonne* (March 2018), respectively (Glud et al., 2021). A total of 13 cores were analyzed in this study, including 4 Kermadec

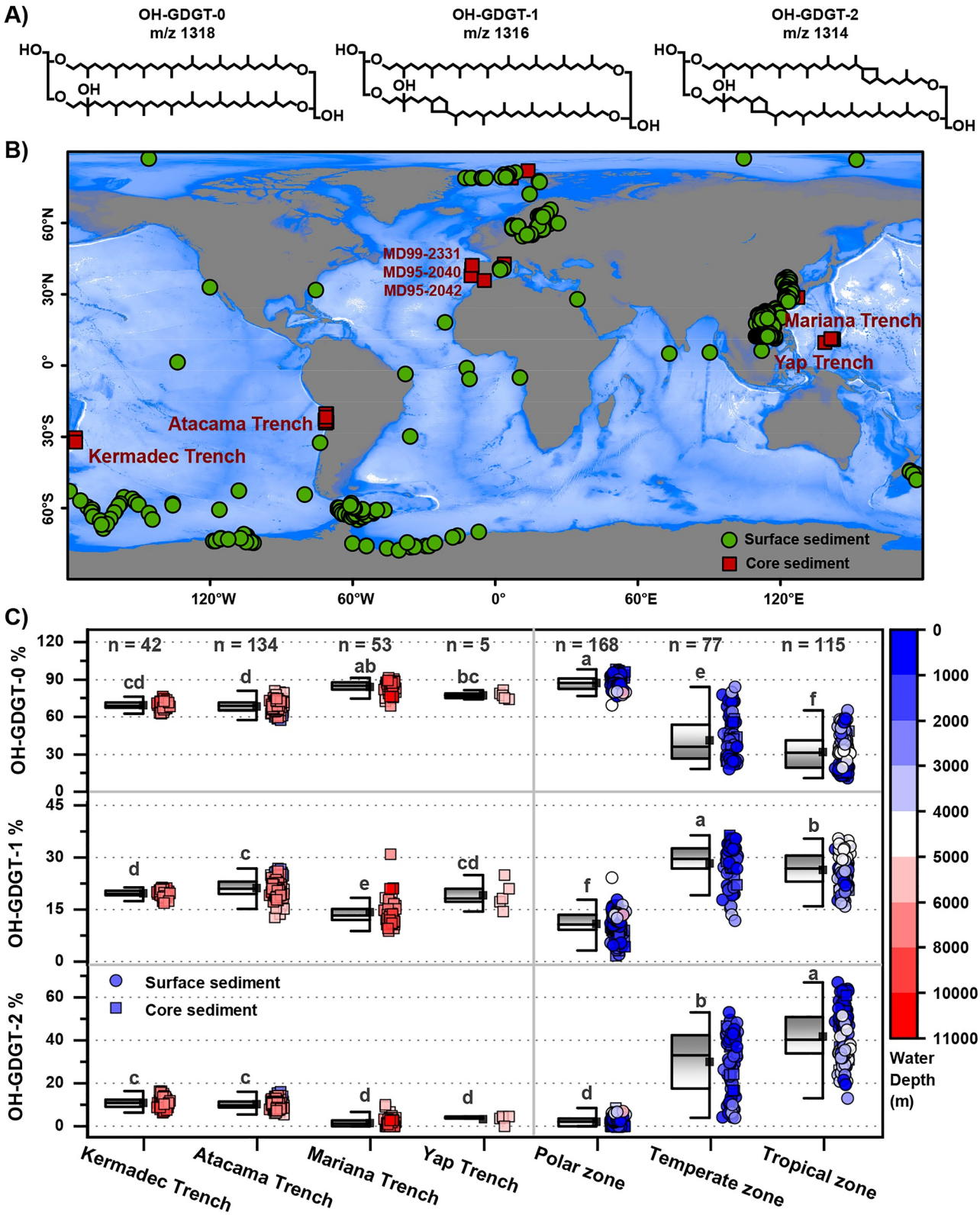

Figure 1. (a) Molecular structures of hydroxylated isoprenoid glycerol dialkyl glycerol tetraethers (OH-GDGTs). (b) World map showing sample locations included in the data set (Supporting Information S1). Circle and square symbols indicate surface and core sediments, respectively. (c) Box plot of relative abundance of OH-GDGT-0, 1, and 2 of samples from the Kermadec, Atacama, Mariana, and Yap trenches, as well as from polar, temperate, and tropical regions. Different letters denote significant differences at the $p < 0.05$ level. The black squares represent the mean values.

Trench cores (6,080–9,560 water depth, 25–40 cm core length) and 9 Atacama Trench cores (2,560–8,090 water depth, 10–35 cm core length) (Figure 1b and Figure S1 in Supporting Information S1). These 13 sediment cores were subsampled into a total of 176 individual samples, which were subsequently kept at −20°C until further analysis. Information on the study area and samples is summarized in Supporting Information S1.

2.2. Lipid Analysis

All lipid extraction and analyses were performed following the methodology described in Xiao et al. (2016). Briefly, lipids were first ultrasonically extracted with dichloromethane/methanol (3:1, v:v) from homogenous freeze-dried samples. The extracts were separated into nonpolar and polar fractions over silica gel columns by hexane and dichloromethane/methanol (1:1, v:v), respectively. The latter fraction containing GDGTs was supplemented with standard C_{46}-GTGT (Huguet et al., 2006) and analyzed using an Agilent ultra-high performance liquid chromatography–atmospheric pressure chemical ionization–mass spectrometry (UHPLC–APCI–MS). The detailed instrumental parameters were adopted from Hopmans et al. (2016). Single ion monitoring (SIM) of $[M + H]^+$ was used, targeting *m/z* 1,302.3, 1,300.3, 1,298.3, 1,296.3, 1,292.3, and 743.6. Under APCI conditions, OH-GDGTs are easily dehydrated to give $[M + H\text{-}18]^+$. Thus OH-GDGTs were determined at *m/z* 1,300.3 (OH-GDGT-0), *m/z* 1,298.3 (OH-GDGT-1) and *m/z* 1,296.3 (OH-GDGT-2) (X. Liu et al., 2012) (Figure S2 in Supporting Information S1).

2.3. Data Compilation

We compiled a global data set consisting of fractional abundance of OH-GDGTs and derived parameters of marine surface sediments ($n = 339$) and core sediments (27 cores) (Text S2 and S3 in Supporting Information S1). These sampling sites span a wide area from 179°W to 177°E and from 78°S to 87°N, and the water depth ranges from 3 to 10,908 m. Information on the data set and references are available in Supporting Information S1. SST is annual mean SST extracted from WOA18 0.25° data set (Locarnini et al., 2018).

2.4. Proxy Calculation

The fractional abundance of each OH-GDGT was calculated (Equation 1). RI-OH and RI-OH′ (Equations 2 and 3) used for SST determination were calculated (Lü et al., 2015). In Equations 1–3, [OH-GDGT-X] is the fractional abundance of OH-GDGT-X, where X is 0, 1 or 2.

$$\text{OH-GDGT-X\%} = \frac{[\text{OH-GDGT-X}]}{[\text{OH-GDGT-0}] + [\text{OH-GDGT-1}] + [\text{OH-GDGT-2}]} \quad (1)$$

$$\text{RI-OH} = \frac{[\text{OH-GDGT-1}] + 2^*[\text{OH-GDGT-2}]}{[\text{OH-GDGT-1}] + [\text{OH-GDGT-2}]} \quad (2)$$

$$\text{RI-OH}' = \frac{[\text{OH-GDGT-1}] + 2^*[\text{OH-GDGT-2}]}{[\text{OH-GDGT-0}] + [\text{OH-GDGT-1}] + [\text{OH-GDGT-2}]} \quad (3)$$

3. Results and Discussion

3.1. Distributional Pattern of OH-GDGTs in Trench and Global Sediments

The abundance of sedimentary OH-GDGTs ranged from 2 to 74 ng g^{-1} dry weight (dw) (mean ± standard deviation, 19 ± 18 ng g^{-1} dw; same hereafter) in the Kerdadec Trench, and from 2 to 1,780 ng g^{-1} dw (243 ± 278 ng g^{-1} dw) in the Atacama Trench (Figure S3 in Supporting Information S1). The composition of OH-GDGTs was dominated by OH-GDGT-0 (69 ± 3% and 68 ± 5%, respectively) in both trenches, followed by OH-GDGT-1 (20 ± 1% and 21 ± 3%, respectively) and then OH-GDGT-2 (11 ± 2% and 10 ± 2%, respectively) (Figure 1c). Interestingly, our results exhibited a remarkable resemblance in the OH-GDGT distributions to those observed in the Yap and Mariana trench core sediments (Chen et al., 2020), which also revealed much higher OH-GDGT-0% (77 ± 3% and 84 ± 5%, respectively) than OH-GDGT-1% (19 ± 4% and 14 ± 4%, respectively) and OH-GDGT-2% (3 ± 2% and 2 ± 2%, respectively). Considering the aforementioned trenches span large geographical settings and differ significantly in biogeochemical properties (Zhang et al., 2022), we hypothesize that the predominance of OH-GDGT-0 is a common phenomenon in the hadal zone.

Sedimentary OH-GDGT-0% in the polar regions (87 ± 5%) was much higher than that of the temperate (41 ± 18%) and tropical (27 ± 12%) regions (Figure 1c, Text S3 in Supporting Information S1). In contrast, OH-GDGT-2% in the polar regions (2 ± 2%) was much lower than that of the temperate (30 ± 14%) and tropical (46 ± 10%) regions. Although the Kermadec, Atacama, Yap and Mariana trenches lie in the tropical to temperate regions, their sediments have similar OH-GDGTs compositions to the polar regions (Figure 1c). This is consistent with the Principal Component Analysis results (Figure S4 in Supporting Information S1) showing that the hadal trench sediments were more closely grouped with polar region sediments.

The inter-trench comparison reveals that OH-GDGT-0% in the Mariana (84 ± 5%) and Yap (77 ± 3%) trench core sediments is higher than that of the Kermadec (69 ± 3%) and Atacama (68 ± 5%) trench core sediments (Figure S1 in Supporting Information S1). In the Atacama Trench, the trench axis sites have lower OH-GDGT-0% (A2, 71 ± 2%; A3, 68 ± 2%; A4, 71 ± 1%; A5, 71 ± 2%; A6, 71 ± 2%; A10, 65 ± 3%) than the oceanward slope sites (A7, 74 ± 5%), and higher or comparable OH-GDGT-0% than the landward slope sites (A1, 61 ± 1%; A9, 64 ± 2%). In the Kermadec Trench, the trench axis sites have slightly higher or comparable OH-GDGT-0% (K3, 73 ± 2%; K4, 68 ± 1%; K6, 70 ± 1%) than the oceanward abyssal site (K7, 67 ± 3%). In the Mariana Trench, the Challenger Deep site has the lowest OH-GDGT-0% (LR1, 76 ± 1%) compared to the surrounding shallow sites (B1, 80 ± 5%; B6, 86 ± 3%; B9, 83 ± 5%; B10, 87 ± 2%).

The above results demonstrate complex distributional patterns of OH-GDGTs within trench interiors, influenced by multiple factors like seawater temperature, water depth and depositional processes, which are discussed in the following section.

3.2. Effect of Water Depth on OH-GDGT Distributions

At the global scale, SST has a strong negative correlation with OH-GDGT-0% ($R^2 = 0.67$, $n = 284$, $p < 0.001$, Figure 2a), but positive correlations with OH-GDGT-1% ($R^2 = 0.57$, $n = 284$, $p < 0.001$), and OH-GDGT-2% ($R^2 = 0.62$, $n = 284$, $p < 0.001$), suggesting that temperature is a controlling factor on OH-GDGTs. Note that these correlation analyses were based on surface sediments and core-top sediments only, to mitigate potential errors arising from the comparison of OH-GDGTs in older sediments with modern SSTs (Text S3 in Supporting Information S1). Given the strongest correlation between OH-GDGT-0% and SST, and significant or even predominant proportions of OH-GDGT-0 in deep-sea sediments, we recommend using RI-OH′ for SST rather than RI-OH because the former includes OH-GDGT-0 in the denominator. Indeed, RI-OH′ has a slightly stronger linear correlation with SST ($R^2 = 0.73$, $n = 365$, $p < 0.001$, Figure 2a) than RI-OH ($R^2 = 0.67$, $n = 299$, $p < 0.001$, Figure S5, Text S3 in Supporting Information S1). The superiority of RI-OH′ over RI-OH was also emphasized by Davtian and Bard (2023), who highlighted the impact of the latter on the abrupt variability in reconstructed SSTs.

The individual OH-GDGT compounds and RI-OH′ versus SST correlations revealed considerable scatter for the hadal trench sediments. Specifically, in the order of Kermadec, Atacama, Mariana, and Yap trenches, the estimation error in OH-GDGT-0% was 19 ± 4%, 16 ± 5%, 53 ± 5%, and 47 ± 3%, respectively (Figure 2a); while their respective estimation error in OH-GDGT-2% was 16 ± 3%, 15 ± 2%, 39 ± 2%, and 18 ± 19%. Correspondingly, the fitting values display higher RI-OH′ estimates than measured values for the hadal trench sediments, with the deviation of 0.35 ± 0.07, 0.31 ± 0.07, 0.92 ± 0.07, and 0.84 ± 0.03, respectively. These discrepancies cause underestimation of SSTs (ca. 5–22°C) using RI-OH′ transfer functions, as well as overestimation of depth-integrated water column temperature and bottom water temperature by ca. 4–12°C (Figure S6 in Supporting Information S1). In the South China Sea, RI-OH′ also showed a decreasing trend with increasing water depth ($R^2 = 0.63$, $n = 109$, $p < 0.001$) (Lü et al., 2015; Wei et al., 2020; Yang, 2017; Yang et al., 2018), and the sediments with water depth >1,000 m have significantly ($p < 0.001$) lower RI-OH′ (0.57 ± 0.10 vs. 1.07 ± 0.19) values than the sediments with water depth <1,000 m (Figure S7 in Supporting Information S1).

The substantial scatter in OH-GDGT-0, 1% and 2% and RI-OH′ versus SST correlations, especially for sediments from the deep oceans, reveals a significant water depth effect on OH-GDGTs-based paleothermometers. In deep oceans, OH-GDGT-producing organisms, mainly Thaumarchaeota (X. Liu et al., 2012), have to adapt to ambient cold deep water compared to the shallow water counterparts. Nunoura et al. (2015) reported that the relative abundance of pelagic Thaumarchaeota varied between 10% and 80% in bathyal, abyssal and hadal water columns of the Mariana Trench region. In sediments of the Mariana, Massua and New Britain trenches, Xu

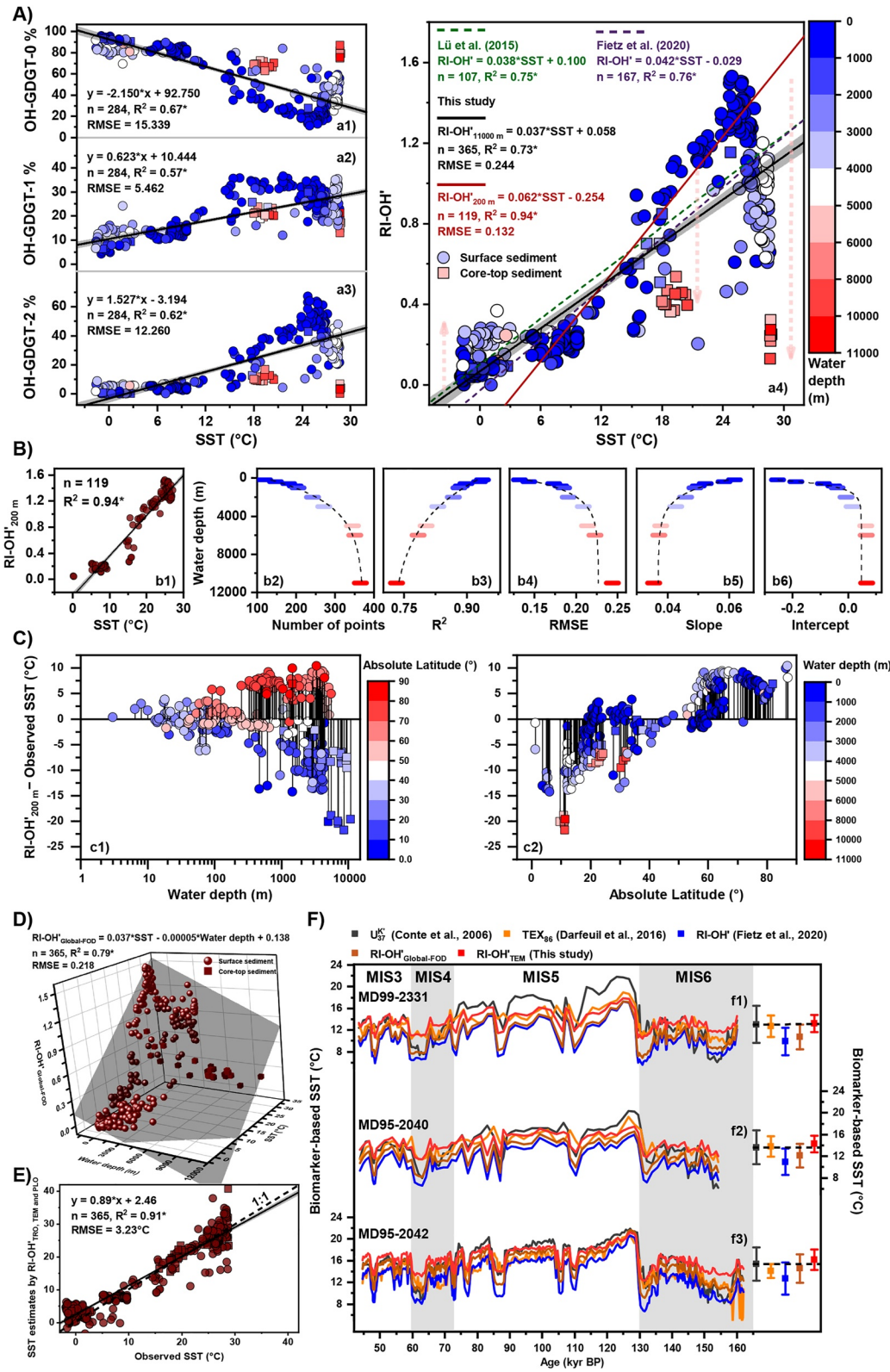

Figure 2.

et al. (2020b) found that benthic Thaumarchaeota dominated the archeal communities (80 ± 30%) and suggested that benthic Thaumarchaeota were a major source of intact polar lipids preserved in trench sediments. Similarly, Schauberger et al. (2021) showed that benthic Thaumarchaeota were overwhelmingly dominant in the archeal data set in core sediments of the Kermadec and Atacama trenches. In addition, Villanueva et al. (2015) observed that the distributional changes of isoGDGTs in the Arabian Sea coincide with the water depth niches occupied by shallow- and deep-water derived pelagic Thaumarchaeota. Taking into account these findings along with our results, we suggest that sedimentary OH-GDGTs in deep ocean sediments may incorporate significant contributions from deep water organisms, as well as possible contributions from benthic organisms. With increasing water depth, archaea would incline to produce more acyclic OH-GDGT-0 compound to adapt to the decreasing water temperature (Figure 2a). Given the greater resistance of OH-GDGT-0 compared to OH-GDGT-1 and 2 (X. Liu et al., 2012), preferential degradation may also contribute to higher OH-GDGT-0% in the deep ocean. However, considering the strong linkage between OH-GDGTs and temperature, we suggest that temperature remains the primary factor.

The contribution of OH-GDGTs from deep water and/or sedimentary in-situ production can be high enough to overprint the signatures from shallow water, causing severe SST bias based on OH-GDGTs, as we observed in the deepest oceanic trenches and the South China Sea deep basin. Many studies have demonstrated that Thaumarchaeota thriving in deeper waters produce a higher abundance of isoGDGT-2 relative to isoGDGT-3 ([2]/[3] ratio) (e.g., Kim et al., 2015; Taylor et al., 2013). However, Xu et al. (2020a) showed that the reconstructed SSTs using TEX_{86} of core-top sediments of the Kermadec and Atacama trenches align relatively well with observed in situ SSTs. It is likely due to both isoGDGT-2 and 3 appear in the numerator and denominator of TEX_{86}, which offsets the water depth effect on TEX_{86}-SSTs (Rattanasriampaipong et al., 2022). Thus, RI-OH′ is more influenced by water depth than TEX_{86}. The Mariana and Yap trenches, which yield severe underestimates of RI-OH′-derived SSTs, are also characterized by higher isoGDGT [2]/[3] ratios compared to the Kermadec and Atacama trenches (Chen et al., 2020; Xu et al., 2020a). This observation suggests a potential connection between isoGDGTs and OH-GDGTs, indicating that they may share the same producers.

3.3. Latitudinal Variation in the Effect of Water Depth

The weighed contribution of water depth effect on OH-GDGTs varies spatiotemporally (Figure S8 in Supporting Information S1). With a large temperature difference of up to 30°C between surface and deep waters in the tropical regions, the contribution of OH-GDGTs from deep water dwelling archaea can cause a great underestimation in sedimentary OH-GDGT-derived SST signatures. Whereas in high latitude regions, there is a minor difference between surface and deep water temperature, and consequently, SST estimates derived using OH-GDGTs in deep and shallow water sediments may be similar. In polar oceans with permanent sea-ice condition that have annual mean SSTs <2°C, deep water-dwelling archaea could even produce relatively less OH-GDGT-0% and cause a minor overestimate in sedimentary OH-GDGT-derived SST signatures (Lamping et al., 2021) (Figure 2a), because the deep water (2–4°C) is warmer than the surface water. Despite the relatively small temperature offsets between surface and deep water in modern polar regions, caution should still be exercised in applying OH-GDGTs for geological studies in polar regions, because polar SSTs could be much warmer on geological timescales, for example, Southern Ocean SST was up to 20°C during the middle Cretaceous (Jenkyns et al., 2004). The contrasting pattern of OH-GDGT distributional change with increasing water depth between tropical and polar regions implies that water depth primarily influences OH-GDGTs through its association with water temperature rather than hydrostatic pressure. However, since hydrostatic pressure is known to alter bacterial membrane lipids (Yano et al., 1998), how it affects archaea-derived OH-GDGT distributions remains largely unknown and warrants further investigation.

Figure 2. (a) Linear regression between sea surface temperature (SST) and relative abundance of OH-GDGT-0, 1, and 2 (a1–a3), and RI-OH′ (a4). Circle and square symbols indicate surface and core-top sediments, respectively. Regression line (black) and 95% confidence intervals (gray band) are shown. $*p < 0.001$. The pink arrows indicate the differential water depth effect depending on the latitude. (b) Linear regression between SST and $RI\text{-}OH'_{200\,m}$ (b1); variation of linear regression parameters, including sample numbers (b2), R^2 (b3), residual mean standard error (b4), linear slope (b5), and intercept (b6), with increasing water depth. (c) Variation of SST residuals estimated by subtracting observed SSTs from $RI\text{-}OH'_{200\,m}$ SST estimates with respect to water depth (c1) and latitude (c2). (d) Three-dimensional regression between RI-OH′, water depth and SST. (e) Linear regression between observed SST and SST estimated by $RI\text{-}OH'_{TRO,TEM,POL}$. (f) $U^{K'}_{37}$-(Conte et al., 2006), TEX_{86}-(Darfeuil et al., 2016), RI-OH′-(Fietz et al., 2020), $RI\text{-}OH'_{Global\text{-}FOD}$- and $RI\text{-}OH'_{TEM}$-SST profiles and their differences from Iberian Margin cores MD99-2331, MD95-2040, and MD95-2042 during the 160–45 kyr BP period. Biomarkers data were cited from Davtian et al. (2021).

3.4. Potential Effect of Export Dynamics on OH-GDGT Distributions

In addition to water depth and SST, export dynamics that affect material transport may also have an impact on OH-GDGT distributions. The core sites of the Mariana, Yap, Kermadec, and Atacama trench regions have average water depths of 7,840 ± 1,820, 5,060, 8,620 ± 1,470, and 6,600 ± 1,940 m, respectively. Although the Mariana and Yap trenches underlie warmer surface waters (ca. 28°C) than the Kermadec and Atacama trenches (ca. 20°C), the former exhibit higher OH-GDGT-0% than the latter (84 ± 5% and 77 ± 3% vs. 69 ± 3% and 68 ± 5%) and lower RI-OH′ values (0.18 ± 0.07 and 0.26 ± 0.03 vs. 0.42 ± 0.06 and 0.42 ± 0.07%). This inconsistency with the global trend suggests higher weighed contributions of OH-GDGTs from deep water archaea in the Mariana and Yap trenches. In contrast, the Kermadec and Atacama trenches underlie higher productive waters and are relatively closer to landmasses, leading to larger and more effective downward export of surface and subsurface materials (e.g., packaging onto fecal pellets, terrestrial substrates or marine snow aggregates; e.g., Wuchter et al., 2005). From this perspective, sedimentary OH-GDGTs may record the events that impact export dynamics, such as sea-level change, marine eutrophication, and lateral transport from submarine landslides.

Input of materials through lateral advection is significant in the hadal zone due to the unique V-shaped topographical feature and frequent mass-wasting events (Glud et al., 2021; M. Liu et al., 2021; Xiao et al., 2020b; Zabel et al., 2022). In the Atacama Trench, all the trench axis sites have lower OH-GDGT-0%, higher RI-OH′, and higher $\text{RI-OH}'_{\text{TEM}}$ SST estimates compared to the adjacent oceanward abyssal plain site (Figure S1 in Supporting Information S1). This may be due to lateral transport, which transports more materials from the upper ocean into the trench bottom. A similar phenomenon was observed in the Mariana Trench, with the Challenger Deep site exhibiting lower OH-GDGT-0% and higher RI-OH′ values than all shallower sites (Figure S1 in Supporting Information S1). Accordingly, the largest negative offset between observed SSTs and $\text{RI-OH}'_{\text{TRO}}$ SST estimates was observed in the Challenger Deep site (Figure S6 in Supporting Information S1), indicating significant lateral transport there. These results are consistent with findings revealed from sedimentological and geochemical data (Luo et al., 2017; Oguri et al., 2022; Xu et al., 2021; Zabel et al., 2022). Quantitatively assessing the potential effect of export dynamics on OH-GDGT signals is challenging, especially on a global scale. Considering the primary significance of the temperature effect, our proposed calibrations in the subsequent section do not specifically evaluate the influence of export dynamics.

3.5. Implications for Paleoenvironmental Reconstructions

To disentangle the effects of temperature and water depth on OH-GDGT-based proxies, we applied linear regression fits between RI-OH′ and SST using samples from different water depths (Figure 2b and Figure S9, Table S1 in Supporting Information S1). Considering the sample size (n = 365) and the water depth range (0–11,000 m), we fitted RI-OH′ at 200 m water depth bin for the epipelagic and mesopelagic zones (0–1,000 m, n = 205), 1,000 m bin for the bathypelagic and abyssopelagic zones (1,000–6,000 m, n = 146), and 5,000 m bin for the hadal zone (6,000–11,000 m, n = 14). With increasing water depth, the coefficient of determination (R^2) of RI-OH′ – SST calibrations decreased monotonically from 0.94 to 0.73, and the corresponding residual mean standard error (RMSE) increased monotonically from 0.13 to 0.24 (Figure 2b), supporting the argument that water depth could cause bias in RI-OH" reconstructed SSTs. When water depth is less than 1,000 m, the R^2 values were >0.88, and the associated RMSE values were <0.19. However, when the water depth exceeds 1,000 m, the R^2 values decreased from 0.88 to 0.73 and RMSE increased from 0.19 to 0.24, suggesting that RI-OH′ should be used with great caution for deep-sea sediments. Currently, the number of RI-OH′ data from >1,000 m water depth is fewer than that from <1,000 m (160 vs. 205), and further investigation for deep-sea sediments is needed.

Based on the global data set, we established $\text{RI-OH}'_{\text{200,400,600,800 and 1,000 m}}$-SST calibrations that are suitable for sediments with water depth less than 200, 400, 600, 800 and 1,000 m, respectively (Equations 4–5 were shown as examples, and the rest were listed in Table S1 in Supporting Information S1). Sedimentary archives preserved in continental shelves with high sedimentation rate are important media for paleoclimatic research, especially for the Late Cenozoic. For continental shelf sediments, $\text{RI-OH}'_{\text{200 m}}$ could yield more accurate SST estimates than Fietz et al. (2020) and Lü et al. (2015) calibrations, because the latter may be influenced by water depth. For instance, Fietz et al. (2020) calibration is similar to $\text{RI-OH}'_{\text{4,000 m}}$, and tends to overestimate SST signals (Figure S10 in Supporting Information S1). When continental shelf sediments have RI-OH′ values of 1.2, SST estimates using Fietz et al. (2020) calibration are ca. 5°C higher than our $\text{RI-OH}'_{\text{200 m}}$ estimates (see red dashed lines in Figure S10 in Supporting Information S1). SST estimation error of $\text{RI-OH}'_{\text{200 m}}$ (2.1°C) is slightly smaller than

that of TEX_{86} (2.5°C of Kim et al., 2010), and much smaller than that of RI-OH′ (6.0°C of Fietz et al., 2020), and Methylation and Cyclization of Branched Tetraethers (MBT/CBT; 5.0°C of Peterse et al., 2012, and 4.8°C of De Jonge et al., 2014). Compared to TEX_{86}, RI-OH′ has an advantage in less sensitivity for terrestrial influence, which is important for SST reconstructions in regions where terrestrial input is significant. Therefore, we propose that $RI\text{-}OH'_{200\,m}$ is promising to quantitatively reconstruct paleo-SSTs for continental shelf sediments. Note the influence of salinity on $RI\text{-}OH'_{200\,m}$ should be considered since the salinity in coastal areas can change significantly (Sinninghe Damste et al., 2022). In addition, $RI\text{-}OH'_{400,600,800\text{ and }1{,}000\,m}$, which are also less affected by water depth, are promising paleothermometers for mesopelagic sediments (water depth <1,000 m).

Taking into consideration that sedimentary OH-GDGTs are primarily controlled by SST and water depth, and that $RI\text{-}OH'_{200\,m}$ is minimally affected by water depth, the offset between observed SSTs and $RI\text{-}OH'_{200\,m}$ SST estimates may reflect the degree of water depth impact. Notably, we have observed significantly larger SST residuals in deep ocean sediments compared to shallow ocean sediments (Figure 2c). Moreover, the SST residuals reveal smaller positive values at high latitudes and considerably larger negative values at low latitudes, again demonstrating that the effect of water depth on sedimentary OH-GDGTs varies depending on latitudinal regions.

$$\mathrm{SST} = 15.2^{*}\mathrm{RI\text{-}OH}'_{200\,m} + 5.0 \left(n = 119, R^2 = 0.94, p < 0.001, \mathrm{RMSE} = 2.1°\mathrm{C}\right) \quad (4)$$

$$\mathrm{SST} = 18.0^{*}\mathrm{RI\text{-}OH}'_{1000\,m} + 2.2 \left(n = 205, R^2 = 0.88, p < 0.001, \mathrm{RMSE} = 3.5°\mathrm{C}\right) \quad (5)$$

$$\mathrm{SST} = 21.2^{*}\mathrm{RI\text{-}OH}'_{\mathrm{Global-FOD}} + 0.0013^{*}\mathrm{Water\ depth} - 0.3 \left(n = 365, R^2 = 0.79, p < 0.001, \mathrm{RMSE} = 5.2°\mathrm{C}\right) \quad (6)$$

$$\mathrm{SST} = 15.2^{*}\mathrm{RI\text{-}OH}'_{\mathrm{TRO}} + 0.0029^{*}\mathrm{Water\ depth} + 5.0 \quad (7)$$

$$\mathrm{SST} = 15.2^{*}\mathrm{RI\text{-}OH}'_{\mathrm{TEM}} + 0.0011^{*}\mathrm{Water\ depth} + 5.0 \quad (8)$$

$$\mathrm{SST} = 15.2^{*}\mathrm{RI\text{-}OH}'_{\mathrm{POL}} - 0.0018^{*}\mathrm{Water\ depth} + 5.0 \quad (9)$$

Given the fact that many sediment cores, like those drilled by International Ocean Discovery Program, are mainly located in deep ocean sites, it is important to expand the applicability of RI-OH′ in deep oceans. To assess both temperature and water depth effects on RI-OH′, we plotted RI-OH′ against SST and water depth using global samples with a full-ocean-depth range (0–11,000 m; $RI\text{-}OH'_{\mathrm{Global-FOD}}$) in a three-dimensional scatter plot (Figure 2d). The calibration (Equation 6, $R^2 = 0.79$, $n = 365$, $p < 0.001$) reveals that a 1,000 m increase in water depth will cause a 1.3°C increase in reconstructed temperature. This equally-weighed evaluation of water depth effect at the global scale, however, may result in an underestimation for the tropical regions and an overestimation for the polar regions. Therefore, we further established $RI\text{-}OH'_{\mathrm{TRO,TEM,POL}}$ (Equations 7–9) to separately evaluate the water depth effect for different regions (Text S4 in Supporting Information S1). Our results show that a 1,000 m increase in water depth will lead to a 2.9, 1.1, and −1.8°C change in estimated temperature for the tropical, temperate, and polar regions, respectively. SST estimates by $RI\text{-}OH'_{\mathrm{TRO,TEM,POL}}$ are in close agreement with observed SSTs ($R^2 = 0.91$, $n = 365$, $p < 0.001$, Figure 2e). A limitation of these calibrations for deep oceans is their inability to account for the potential variability in contributions of OH-GDGTs from different water depths during geological periods. This limitation arises from the assumption of a constant impact of water depth in our calibrations.

In order to test the validity of our RI-OH′ calibrations at the geological timescale, we compiled the paleo-SST data in Davtian et al. (2021) that high-resolution profiles of $U^{K'}_{37}$ (C_{37} ketone unsaturation ratio), TEX_{86} and RI-OH′ are available in three sediment cores from the Iberian Margin, spanning the period of marine isotope stages 3–6. $U^{K'}_{37}$ is a robust SST indicator because it is sourced from haptophytes that predominantly inhabit surface waters (Conte et al., 2006). These indexes exhibit similar glacial-interglacial temperature cycles. However, RI-OH′-derived SSTs using Fietz et al. (2020) calibration are significantly lower than those estimated by $U^{K'}_{37}$, with average offsets of 2.6, 2.7, and 3.1°C respectively for cores MD95-2040, MD95-2042, and MD99-2331 (Figure 2f), larger than $U^{K'}_{37}$-$RI\text{-}OH'_{\mathrm{Global-FOD}}$ SST offsets (1.5, 0.8, and 2.3°C, respectively) and $U^{K'}_{37}$-$RI\text{-}OH'_{\mathrm{TEM}}$ SST offsets (−0.7, −0.7 and −0.2°C, respectively). Similarly, RI-OH′-derived SSTs exhibit better agreement with the temperature estimates derived from TEX_{86} when using our proposed calibrations (Figure 2f). Furthermore, our calibrations demonstrate good performance when applied to the OH-GDGT data reported by Davtian and Bard (2023) (Figure S11 in Supporting Information S1).

Since OH-GDGTs were influenced by water depth, the variation of water depth over geological time may also exerts influence in the interpretation of RI-OH′. However, such effect would be minor. As discussed earlier, a 1,000 m increase in water depth would cause a 2.9°C increase or 1.8°C decrease in estimated temperature. The variation of global mean sea level is typically less than 300 m since the Early Jurassic (the earliest known record of GDGTs) (Miller et al., 2005; Robinson et al., 2017), corresponding to a SST deviation of <1.0°C; whereas the variation of SSTs since the Early Jurassic can reach up to 20°C (Veizer & Prokoph, 2015). In this perspective, the influence of water depth variation on RI-OH′ for deep-sea sediments would be insignificant compared to that of SST and absolute water depth. However, it should be noted that caution is necessary when dealing with paleostudies that exhibit great variations in paleowater depths, likely due to factors such as sea-floor spreading and crustal subsidence (Ehlers & Jokat, 2013). Overall, our findings support the use of RI-OH′ as an effective indicator of SST variability over geological time, allowing for relatively accurate estimation of past SSTs when the modern water depth of the study site is known.

4. Conclusions

The Kermadec, Atacama, Mariana, and Yap trench sediments were characterized by a strong dominance of OH-GDGT-0 and low RI-OH′ values. This phenomenon was also observed in other deep-sea sediments, attributed to a ubiquitous contribution of deep water organisms to the sedimentary OH-GDGT pool. These findings emphasize the significant influence of water depth on OH-GDGTs and underscore the need to consider this factor when reconstructing paleo-SSTs. By developing improved and global OH-GDGT-based paleothermometers, our study offers a powerful tool for accurately estimating paleo-SSTs.

Data Availability Statement

All the original data have been deposited publicly to the repository of Zenodo (https://doi.org/10.5281/zenodo.7114938). All the supporting data can be found in the cited references (Chen et al., 2020; Davtian & Bard, 2023; Davtian et al., 2019, 2021; Fietz et al., 2013, 2016; Huguet et al., 2013; Kaiser & Arz, 2016; Kremer et al., 2018; Lamping et al., 2021; L. Liu et al., 2022; Lü et al., 2015; Morcillo-Montalba et al., 2021; Sinninghe Damste et al., 2022; Wei et al., 2020; Yang, 2017; Yang et al., 2018).

Acknowledgments
We thank Drs. Susanne Fietz and Jerome Kaiser for providing previously published data. This research was supported by the State Key R&D project of China Grant (2018YFA0605800), the National Natural Science Foundation of China (42206040, 42276033, 41976030), the Danish National Research Foundation Grant DNRF145 via the Danish Center for Hadal Research, and the Shanghai Sheshan National Geophysical Observatory (Grant 2020Z01). The voyages were made possible by the HADES-ERC Advanced Grant (669947), the Coasts & Oceans Centre of New Zealand's National Institute of Water & Atmospheric Research (TAN1711).

References

Chen, Z., Li, J., Li, X., Chen, S., Dasgupta, S., Bai, S., et al. (2020). Characteristics and implications of isoprenoid and hydroxy tetraether lipids in hadal sediments of Mariana and Yap Trenches. *Chemical Geology*, *551*, 119742. https://doi.org/10.1016/j.chemgeo.2020.119742

Conte, M. H., Sicre, M.-A., Rühlemann, C., Weber, J. C., Schulte, S., Schulz-Bull, D., & Blanz, T. (2006). Global temperature calibration of the alkenone unsaturation index (UK'37) in surface waters and comparison with surface sediments. *Geochemistry, Geophysics, Geosystems*, *7*(2), Q02005. https://doi.org/10.1029/2005GC001054

Darfeuil, S., Ménot, G., Giraud, X., Rostek, F., Tachikawa, K., Garcia, M., & Bard, É. (2016). Sea surface temperature reconstructions over the last 70 kyr off Portugal: Biomarker data and regional modeling. *Paleoceanography*, *31*(1), 40–65. https://doi.org/10.1002/2015PA002831

Davtian, N., & Bard, E. (2023). A new view on abrupt climate changes and the bipolar seesaw based on paleotemperatures from Iberian Margin sediments. *Proceedings of the National Academy of Sciences*, *120*(12), e2209558120. https://doi.org/10.1073/pnas.2209558120

Davtian, N., Bard, E., Darfeuil, S., Menot, G., & Rostek, F. (2021). The Novel hydroxylated tetraether index RI-OH' as a sea surface temperature proxy for the 160-45 ka BP period off the Iberian margin. *Paleoceanography and Paleoclimatology*, *36*(3), e2020PA004077. https://doi.org/10.1029/2020pa004077

Davtian, N., Ménot, G., Fagault, Y., & Bard, E. (2019). Western Mediterranean sea paleothermometry over the last glacial cycle based on the Novel RI-OH index. *Paleoceanography and Paleoclimatology*, *34*(4), 616–634. https://doi.org/10.1029/2018PA003452

De Jonge, C., Hopmans, E. C., Zell, C. I., Kim, J.-H., Schouten, S., & Sinninghe Damsté, J. S. (2014). Occurrence and abundance of 6-methyl branched glycerol dialkyl glycerol tetraethers in soils: Implications for palaeoclimate reconstruction. *Geochimica et Cosmochimica Acta*, *141*, 97–112. https://doi.org/10.1016/j.gca.2014.06.013

Ehlers, B.-M., & Jokat, W. (2013). Paleo-bathymetry of the northern North Atlantic and consequences for the opening of the Fram strait. *Marine Geophysical Researches*, *34*(1), 25–43. https://doi.org/10.1007/s11001-013-9165-9

Elling, F. J., Könneke, M., Lipp, J. S., Becker, K. W., Gagen, E. J., & Hinrichs, K.-U. (2014). Effects of growth phase on the membrane lipid composition of the thaumarchaeon Nitrosopumilus maritimus and their implications for archaeal lipid distributions in the marine environment. *Geochimica et Cosmochimica Acta*, *141*, 579–597. https://doi.org/10.1016/j.gca.2014.07.005

Elling, F. J., Könneke, M., Nicol, G. W., Stieglmeier, M., Bayer, B., Spieck, E., et al. (2017). Chemotaxonomic characterisation of the thaumarchaeal lipidome. *Environmental Microbiology*, *19*(7), 2681–2700. https://doi.org/10.1111/1462-2920.13759

Fietz, S., Ho, S. L., & Huguet, C. (2020). Archaeal membrane lipid-based paleothermometry for applications in polar oceans. *Oceanography*, *33*(2), 104–114. https://doi.org/10.5670/oceanog.2020.207

Fietz, S., Ho, S. L., Huguet, C., Rosell-Mele, A., & Martinez-Garcia, A. (2016). Appraising GDGT-based seawater temperature indices in the Southern Ocean. *Organic Geochemistry*, *102*, 93–105. https://doi.org/10.1016/j.orggeochem.2016.10.003

Fietz, S., Huguet, C., Rueda, G., Hambach, B., & Rosell-Mele, A. (2013). Hydroxylated isoprenoidal GDGTs in the Nordic seas. *Marine Chemistry*, *152*, 1–10. https://doi.org/10.1016/j.marchem.2013.02.007

Glud, R. N., Berg, P., Thamdrup, B., Larsen, M., Stewart, H. A., Jamieson, A. J., et al. (2021). Hadal trenches are dynamic hotspots for early diagenesis in the deep sea. *Communications Earth & Environment*, *2*(1), 21. https://doi.org/10.1038/s43247-020-00087-2

Glud, R. N., Wenzhofer, F., Middelboe, M., Oguri, K., Turnewitsch, R., Canfield, D. E., & Kitazato, H. (2013). High rates of microbial carbon turnover in sediments in the deepest oceanic trench on Earth. *Nature Geoscience*, *6*(4), 284–288. https://doi.org/10.1038/NGEO1773

Harning, D. J., Holman, B., Woelders, L., Jennings, A. E., & Sepúlveda, J. (2023). Biomarker characterization of the North water Polynya, Baffin Bay: Implications for local sea ice and temperature proxies. *Biogeosciences*, *20*(1), 229–249. https://doi.org/10.5194/bg-20-229-2023

Hopmans, E. C., Schouten, S., & Damsté, J. S. S. (2016). The effect of improved chromatography on GDGT-based palaeoproxies. *Organic Geochemistry*, *93*, 1–6. https://doi.org/10.1016/j.orggeochem.2015.12.006

Huguet, C., Fietz, S., & Rosell-Mele, A. (2013). Global distribution patterns of hydroxy glycerol dialkyl glycerol tetraethers. *Organic Geochemistry*, *57*, 107–118. https://doi.org/10.1016/j.orggeochem.2013.01.010

Huguet, C., Hopmans, E. C., Febo-Ayala, W., Thompson, D. H., Damste, J. S. S., & Schouten, S. (2006). An improved method to determine the absolute abundance of glycerol dibiphytanyl glycerol tetraether lipids. *Organic Geochemistry*, *37*(9), 1036–1041. https://doi.org/10.1016/j.orggeochem.2006.05.008

Inglis, G. N., & Tierney, J. E. (2020). *The TEX86 paleotemperature proxy*. Cambridge University Press. https://doi.org/10.1017/9781108846998

Jenkyns, H. C., Forster, A., Schouten, S., & Sinninghe Damsté, J. S. (2004). High temperatures in the late Cretaceous Arctic ocean. *Nature*, *432*(7019), 888–892. https://doi.org/10.1038/nature03143

Kaiser, J., & Arz, H. W. (2016). Sources of sedimentary biomarkers and proxies with potential paleoenvironmental significance for the Baltic Sea. *Continental Shelf Research*, *122*, 102–119. https://doi.org/10.1016/j.csr.2016.03.020

Kang, S., Shin, K.-H., & Kim, J.-H. (2017). Occurrence and distribution of hydroxylated isoprenoid glycerol dialkyl glycerol tetraethers (OH-GDGTs) in the Han River system, South Korea. *Acta Geochimica*, *36*(3), 367–369. https://doi.org/10.1007/s11631-017-0165-3

Kim, J.-H., Schouten, S., Rodrigo-Gámiz, M., Rampen, S., Marino, G., Huguet, C., et al. (2015). Influence of deep-water derived isoprenoid tetraether lipids on the TEX86H paleothermometer in the Mediterranean Sea. *Geochimica et Cosmochimica Acta*, *150*, 125–141. https://doi.org/10.1016/j.gca.2014.11.017

Kim, J. H., van der Meer, J., Schouten, S., Helmke, P., Willmott, V., Sangiorgi, F., et al. (2010). New indices and calibrations derived from the distribution of crenarchaeal isoprenoid tetraether lipids: Implications for past sea surface temperature reconstructions. *Geochimica et Cosmochimica Acta*, *74*(16), 4639–4654. https://doi.org/10.1016/j.gca.2010.05.027

Kremer, A., Stein, R., Fahl, K., Ji, Z., Yang, Z., Wiers, S., et al. (2018). Changes in sea ice cover and ice sheet extent at the Yermak Plateau during the last 160 ka—Reconstructions from biomarker records. *Quaternary Science Reviews*, *182*, 93–108. https://doi.org/10.1016/j.quascirev.2017.12.016

Lamping, N., Müller, J., Hefter, J., Mollenhauer, G., Haas, C., Shi, X., et al. (2021). Evaluation of lipid biomarkers as proxies for sea ice and ocean temperatures along the Antarctic continental margin. *Climate of the Past*, *17*(5), 2305–2326. https://doi.org/10.5194/cp-17-2305-2021

Liu, L., Guan, H., Xu, L., Sun, Z., & Wu, N. (2022). Paleoclimate records of the middle Okinawa trough since the middle Holocene: Modulation of the low-latitude climate. *Frontiers in Earth Science*, *10*, 799280. https://doi.org/10.3389/feart.2022.799280

Liu, M., Xiao, W., Zhang, Q., Yuan, S., Raymond, P. A., Chen, J., et al. (2021). Substantial accumulation of mercury in the deepest parts of the ocean and implications for the environmental mercury cycle. *Proceedings of the National Academy of Sciences*, *118*(51), e2102629118. https://doi.org/10.1073/pnas.2102629118

Liu, X., Lipp, J. S., Simpson, J. H., Lin, Y.-S., Summons, R. E., & Hinrichs, K.-U. (2012). Mono- and dihydroxyl glycerol dibiphytanyl glycerol tetraethers in marine sediments: Identification of both core and intact polar lipid forms. *Geochimica et Cosmochimica Acta*, *89*, 102–115. https://doi.org/10.1016/j.gca.2012.04.053

Locarnini, M., Mishonov, A. V., Baranova, O. K., Boyer, T. P., Zweng, M. M., Garcia, H. E., et al. (2018). World ocean atlas 2018, volume 1: Temperature.

Lü, X., Chen, J., Han, T., Yang, H., Wu, W., Ding, W., & Hinrichs, K.-U. (2019). Origin of hydroxyl GDGTs and regular isoprenoid GDGTs in suspended particulate matter of Yangtze River Estuary. *Organic Geochemistry*, *128*, 78–85. https://doi.org/10.1016/j.orggeochem.2018.12.010

Lü, X., Liu, X., Elling, F. J., Yang, H., Xie, S., Song, J., et al. (2015). Hydroxylated isoprenoid GDGTs in Chinese coastal seas and their potential as a paleotemperature proxy for mid-to-low latitude marginal seas. *Organic Geochemistry*, *89–90*, 31–43. https://doi.org/10.1016/j.orggeochem.2015.10.004

Luo, M., Gieskes, J., Chen, L., Shi, X., & Chen, D. (2017). Provenances, distribution, and accumulation of organic matter in the southern Mariana Trench rim and slope: Implication for carbon cycle and burial in hadal trenches. *Marine Geology*, *386*(2), 486–498. https://doi.org/10.1016/j.margeo.2017.02.012

Miller, K. G., Kominz, M. A., Browning, J. V., Wright, J. D., Mountain, G. S., Katz, M. E., et al. (2005). The Phanerozoic record of global sea-level change. *Science*, *310*(5752), 1293–1298. https://doi.org/10.1126/science.1116412

Morcillo-Montalba, L., Rodrigo-Gamiz, M., Martinez-Ruiz, F., Ortega-Huertas, M., Schouten, S., & Damste, J. S. S. (2021). Rapid climate changes in the Westernmost Mediterranean (Alboran sea) over the last 35 kyr: New Insights from Four lipid paleothermometers ($U_{37}^{K'}$, TEX_{86}^{H}, RI-OH', and LDI). *Paleoceanography and Paleoclimatology*, *36*(12), e2020PA004171. https://doi.org/10.1029/2020pa004171

Nunoura, T., Takaki, Y., Hirai, M., Shimamura, S., Makabe, A., Koide, O., et al. (2015). Hadal biosphere: Insight into the microbial ecosystem in the deepest ocean on Earth. *Proceedings of the National Academy of Sciences of the United States of America*, *112*(11), E1230–E1236. https://doi.org/10.1073/pnas.1421816112

Oguri, K., Masqué, P., Zabel, M., Stewart, H. A., MacKinnon, G., Rowden, A. A., et al. (2022). Sediment accumulation and carbon burial in Four Hadal Trench systems. *Journal of Geophysical Research: Biogeosciences*, *127*(10), e2022JG006814. https://doi.org/10.1029/2022JG006814

Peterse, F., van der Meer, J., Schouten, S., Weijers, J. W. H., Fierer, N., Jackson, R. B., et al. (2012). Revised calibration of the MBT-CBT paleotemperature proxy based on branched tetraether membrane lipids in surface soils. *Geochimica et Cosmochimica Acta*, *96*, 215–229. https://doi.org/10.1016/j.gca.2012.08.011

Rattanasriampaipong, R., Zhang, Y. G., Pearson, A., Hedlund, B. P., & Zhang, S. (2022). Archaeal lipids trace ecology and evolution of marine ammonia-oxidizing archaea. *Proceedings of the National Academy of Sciences*, *119*(31), e2123193119. https://doi.org/10.1073/pnas.2123193119

Robinson, S. A., Ruhl, M., Astley, D. L., Naafs, B. D. A., Farnsworth, A. J., Bown, P. R., et al. (2017). Early Jurassic North Atlantic sea-surface temperatures from TEX86 palaeothermometry. *Sedimentology*, *64*(1), 215–230. https://doi.org/10.1111/sed.12321

Schauberger, C., Glud, R. N., Hausmann, B., Trouche, B., Maignien, L., Poulain, J., et al. (2021). Microbial community structure in hadal sediments: High similarity along trench axes and strong changes along redox gradients. *ISME Journal*, *15*(12), 3455–3467. https://doi.org/10.1038/s41396-021-01021-w

Schouten, S., Hopmans, E. C., & Sinninghe Damsté, J. S. (2013). The organic geochemistry of glycerol dialkyl glycerol tetraether lipids: A review. *Organic Geochemistry*, *54*, 19–61. https://doi.org/10.1016/j.orggeochem.2012.09.006

Sinninghe Damste, J. S., Warden, L. A., Berg, C., Jürgens, K., & Moros, M. (2022). Evaluation of the distributions of hydroxylated isoprenoidal GDGTs in Holocene Baltic Sea sediments for reconstruction of sea surface temperature: The effect of changing salinity. *Climate of the Past Discussions*, *18*, 1–25. https://doi.org/10.5194/cp-2022-19

Stewart, H. A., & Jamieson, A. J. (2018). Habitat heterogeneity of hadal trenches: Considerations and implications for future studies. *Progress in Oceanography*, *161*, 47–65. https://doi.org/10.1016/j.pocean.2018.01.007

Summons, R. E., Welander, P. V., & Gold, D. A. (2022). Lipid biomarkers: Molecular tools for illuminating the history of microbial life. *Nature Reviews Microbiology*, *20*(3), 174–185. https://doi.org/10.1038/s41579-021-00636-2

Taylor, K. W. R., Huber, M., Hollis, C. J., Hernandez-Sanchez, M. T., & Pancost, R. D. (2013). Re-evaluating modern and Palaeogene GDGT distributions: Implications for SST reconstructions. *Global and Planetary Change*, *108*, 158–174. https://doi.org/10.1016/j.gloplacha.2013.06.011

Veizer, J., & Prokoph, A. (2015). Temperatures and oxygen isotopic composition of Phanerozoic oceans. *Earth-Science Reviews*, *146*, 92–104. https://doi.org/10.1016/j.earscirev.2015.03.008

Villanueva, L., Schouten, S., & Damste, J. S. S. (2015). Depth-related distribution of a key gene of the tetraether lipid biosynthetic pathway in marine Thaumarchaeota. *Environmental Microbiology*, *17*(10), 3527–3539. https://doi.org/10.1111/1462-2920.12508

Wei, B., Jia, G., Hefter, J., Kang, M., Park, E., Wang, S., & Mollenhauer, G. (2020). Comparison of the $U_{37}^{K'}$, LDI, TEX_{86}^{H}, and RI-OH temperature proxies in sediments from the northern shelf of the South China Sea. *Biogeosciences*, *17*(17), 4489–4508. https://doi.org/10.5194/bg-17-4489-2020

Wuchter, C., Schouten, S., Wakeham, S. G., & Sinninghe Damsté, J. S. (2005). Temporal and spatial variation in tetraether membrane lipids of marine Crenarchaeota in particulate organic matter: Implications for TEX86 paleothermometry. *Paleoceanography*, *20*(3), 1–11. https://doi.org/10.1029/2004PA001110

Xiao, W., Wang, Y., Liu, Y., Zhang, X., Shi, L., & Xu, Y. (2020a). Predominance of hexamethylated 6-methyl branched glycerol dialkyl glycerol tetraethers in the Mariana Trench: Source and environmental implication. *Biogeosciences*, *17*(7), 2135–2148. https://doi.org/10.5194/bg-17-2135-2020

Xiao, W., Wang, Y., Zhou, S., Hu, L., Yang, H., & Xu, Y. (2016). Ubiquitous production of branched glycerol dialkyl glycerol tetraethers (brGDGTs) in global marine environments: A new source indicator for brGDGTs. *Biogeosciences*, *13*(20), 5883–5894. https://doi.org/10.5194/bg-13-5883-2016

Xiao, W., Xu, Y., Haghipour, N., Montluçon, D. B., Pan, B., Jia, Z., et al. (2020b). Efficient sequestration of terrigenous organic carbon in the New Britain Trench. *Chemical Geology*, *533*, 119446. https://doi.org/10.1016/j.chemgeo.2019.119446

Xu, Y., Ge, H., & Fang, J. (2018). Biogeochemistry of hadal trenches: Recent developments and future perspectives. *Deep Sea Research Part II: Topical Studies in Oceanography*, *155*, 19–26. https://doi.org/10.1016/j.dsr2.2018.10.006

Xu, Y., Jia, Z., Xiao, W., Fang, J., Wang, Y., Luo, M., et al. (2020). Glycerol dialkyl glycerol tetraethers in surface sediments from three Pacific trenches: Distribution, source and environmental implications. *Organic Geochemistry*, *147*, 104079. https://doi.org/10.1016/j.orggeochem.2020.104079

Xu, Y., Li, X., Luo, M., Xiao, W., Fang, J., Rashid, H., et al. (2021). Distribution, source, and burial of sedimentary organic carbon in Kermadec and Atacama trenches. *Journal of Geophysical Research-Biogeosciences*, *126*(5), e2020JG006189. https://doi.org/10.1029/2020jg006189

Xu, Y., Wu, W., Xiao, W., Ge, H., Wei, Y., Yin, X., et al. (2020b). Intact ether lipids in trench sediments related to archaeal community and environmental conditions in the deepest ocean. *Journal of Geophysical Research-Biogeosciences*, *125*(7), e2019JG005431. https://doi.org/10.1029/2019jg005431

Yang, Y. (2017). *Spatial distribution of microbial lipids in the surface sediments of the South China Sea and the implications for paleoclimate reconstruction* (Master's thesis). China University of Geoscience.

Yang, Y., Gao, C., Dang, X., Ruan, X., Lu, X., Xie, S., et al. (2018). Assessing hydroxylated isoprenoid GDGTs as a paleothermometer for the tropical South China Sea. *Organic Geochemistry*, *115*, 156–165. https://doi.org/10.1016/j.orggeochem.2017.10.014

Yano, Y., Nakayama, A., Ishihara, K., & Saito, H. (1998). Adaptive changes in membrane lipids of Barophilic Bacteria in response to changes in growth pressure. *Applied and Environmental Microbiology*, *64*(2), 479–485. https://doi.org/10.1128/AEM.64.2.479-485.1998

Zabel, M., Glud, R. N., Sanei, H., Elvert, M., Pape, T., Chuang, P. C., et al. (2022). High carbon mineralization rates in subseafloor hadal sediments - result of frequent mass wasting. *Geochemistry, Geophysics, Geosystems*, *23*(9), e2022GC010502. https://doi.org/10.1029/2022GC010502

Zhang, X., Xu, Y., Xiao, W., Zhao, M., Wang, Z., Wang, X., et al. (2022). The hadal zone is an important and heterogeneous sink of black carbon in the ocean. *Communications Earth & Environment*, *3*(1), 25. https://doi.org/10.1038/s43247-022-00351-7

References From the Supporting Information

Danovaro, R., Della Croce, N., Dell'Anno, A., & Pusceddu, A. (2003). A depocenter of organic matter at 7800 m depth in the SE Pacific Ocean. *Deep Sea Research Part I: Oceanographic Research Papers*, *50*(12), 1411–1420. https://doi.org/10.1016/j.dsr.2003.07.001

Jamieson, A. J. (2015). *The hadal zone: Life in the deepest oceans*. Cambridge University Press. https://doi.org/10.1017/CBO9781139061384